

Three-dimensional optical coherence tomography at 1050 nm versus 800 nm in retinal pathologies: enhanced performance and choroidal penetration in cataract patients

Boris Považay
Boris Hermann
Angelika Unterhuber
Bernd Hofer

Cardiff University
School of Optometry and Vision Sciences
Biomedical Imaging Group
Cardiff, Wales, CF24 4LU, United Kingdom
and

Medical University of Vienna
Center for Biomedical Engineering and Physics
Waehringerstrasse 13
Vienna, A-1090, Vienna, Austria

Harald Sattmann

Medical University of Vienna
Center for Biomedical Engineering and Physics
Waehringerstrasse 13
Vienna, A-1090, Vienna, Austria

Florian Zeiler

Rudolf Foundation Clinic Vienna
Department of Ophthalmology
Ludwig Boltzmann Institute
Juchgasse 25
Vienna, A-1030, Vienna, Austria

James E. Morgan

Cardiff University
School of Optometry and Vision Science 1
Biomedical Imaging Group
Cardiff, Wales, CF24 4LU, United Kingdom

Christiane Falkner-Radler

Carl Glittenberg
Susanne Blinder

Rudolf Foundation Clinic Vienna
Department of Ophthalmology
Ludwig Boltzmann Institute
Juchgasse 25
Vienna, A-1030, Vienna, Austria

Wolfgang Drexler

Cardiff University
School of Optometry and Vision Science 1
Biomedical Imaging Group
Cardiff, Wales, CF24 4LU, United Kingdom
and
Medical University of Vienna
Center for Biomedical Engineering and Physics
Waehringerstrasse 13
Vienna, A-1090, Vienna, Austria

Abstract. Frequency domain optical coherence tomography (FD-OCT), based on an all-reflective high-speed In-GaAs spectrometer, operating in the 1050 nm wavelength region for retinal diagnostics, enables high-speed, volumetric imaging of retinal pathologies with greater penetration into choroidal tissue is compared to conventional 800 nm three-dimensional (3-D) ophthalmic FD-OCT systems. Furthermore, the lower scattering at this wavelength significantly improves imaging performance in cataract patients, thereby widening the clinical applicability of ophthalmic OCT. The clinical performance of two spectrometer-based ophthalmic 3-D OCT systems compared in respect to their clinical performance, one operating at 800 nm with 150 nm bandwidth ($\sim 3 \mu\text{m}$ effective axial resolution) and the other at 1050 nm with 70 nm bandwidth ($\sim 7 \mu\text{m}$ effective axial resolution). Results achieved with 3-D OCT at 1050 nm reveal, for the first time, decisive improvements in image quality for patients with retinal pathologies and clinically significant cataract. © 2007 Society of Photo-Optical Instrumentation Engineers. [DOI: 10.1117/1.2773728]

Keywords: optical coherence tomography (OCT); three-dimensional (3-D) retinal imaging; cataract; choroid; penetration; scattering; infrared.

Paper 06331SSR received Nov. 14, 2006; revised manuscript received Feb. 18, 2007; accepted for publication Feb. 27, 2007; published online Sep. 11, 2007.

1 Introduction and Motivation

In recent years, frequency domain optical coherence tomography (FD-OCT),¹⁻⁶ also referred to as spectral or Fourier domain OCT, has proven to combine high speed and ultrahigh resolution imaging.⁷⁻⁹ High-speed, frequency-domain-based optical coherence tomography ophthalmic imaging systems are commonly designed to operate around 800 nm, which allows for several thousand depth scans per second for three-dimensional (3-D) *in vivo* imaging of the human retina with retinal pathologies.^{10,11} In FD-OCT, the interference pattern in the optical frequency spectrum is analyzed to provide both high-sensitivity and high-speed, depth-resolved measurements of the human retina. Time domain (TD) standard¹²⁻¹⁴ and ultrahigh resolution OCT¹⁵⁻¹⁷ have already demonstrated their clinical value as a noncontact diagnostic tool for the evaluation of retinal diseases by providing virtual sections of the retina at high axial resolution. While these techniques have achieved notable successes, they are limited by relatively low signal-to-noise ratios (SNR) and therefore long data acquisition times that make them unsuitable for 3-D retinal imaging.

Address all correspondence to: Wolfgang Drexler, Redwood Building—King Edward VII Avenue, Cathays Park, CF10 3NB, Maindy Road CF24 4LU, Cardiff, Wales, United Kingdom. Tel: +44 29 2078 0230; Fax: +44 29 2078 0231; E-mail: drexlerw@cardiff.ac.uk

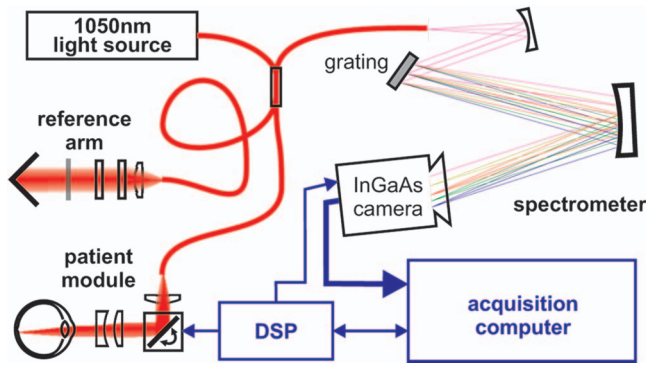


Fig. 1 Schematics of the 1050-nm spatially encoded frequency domain OCT system. The broadband source (emission centered at 1045 nm, bandwidth 70 nm at >20 mW) is interfaced to a fiber-optic interferometer where the first arm is sent to an adjustable reference mirror in a free-space portion including dispersion compensation and an attenuator. The patient module consists of collimation and focusing optics and a 2-D scanner. On its way back, the light from the sample arm is recombined with the reference light, producing a spectral interference pattern that is sent to an all-reflective imaging spectrometer with a reflective planar grating. Processing of the signal from the InGaAs camera is performed with a standard industrial personal computer, while an independent digital signal processor (DSP) serves the position galvanometers and synchronizes the acquisition.

By contrast, high-speed FD-OCT, either in its time-encoded form with high-speed spectrally swept sources and a single detector,^{4,6} or spatially encoded using broadband sources and a spectrometer, is widely expected to revolutionize clinical OCT-based retinal imaging. At present, standard resolution ophthalmic OCT sources commonly operate using 800 nm light sources with up to 30 nm bandwidth and $\sim 10 \mu\text{m}$ axial resolution.¹²⁻¹⁴ Ultrahigh resolution ophthalmic OCT systems

operate in the 650 to 950 nm wavelength range, which falls almost completely outside the sensitivity profile of the human eye to visible light but within the transparency region below the 970 nm water absorption peak or due to limited availability of appropriate light sources. Although 800 nm OCT systems can resolve all major retinal layers, image quality can be severely degraded by abnormal opaque, scattering intraocular media like corneal haze or cataracts. In clinical OCT imaging, cataracts present a significant barrier to the derivation of high-resolution images of the retina. Cataracts degrade the transparency of the lens and remain a major cause of vision loss in both the developed and developing world.¹⁸ Most cataracts are age related, but secondary lens opacities can arise as result of other ocular diseases.

OCT-based retinal imaging is mostly limited by the water absorption¹⁹ of transparent structures such as the cornea, lens, and vitreous that focus light onto the retina. The absorption characteristics of water features two usable regions, separated by an absorption peak at ~ 970 nm; the lower wavelength region covers the visible and the near-range infrared up to ~ 950 nm. The second window is narrower and restricted to ~ 100 nm of bandwidth above 1000 nm. Due to the residual average absorption, the allowed power levels at the cornea according to ANSI or ICNRP standards^{20,21} increase at longer wavelengths by about a factor of four. Despite this drawback and the need for InGaAs spectrometer technology,²² the major advantage of imaging at 1050 nm is that light scattering is significantly reduced (proportional to $\sim \lambda^{-4}$) as demonstrated in measurements from excised tissue samples as based on optical tissue parameters.¹⁹

Due to lower tissue scattering at longer wavelengths, OCT imaging at 1050 nm has already shown deeper penetration into tissue,^{19,23-25} allowing for visualization of structures be-

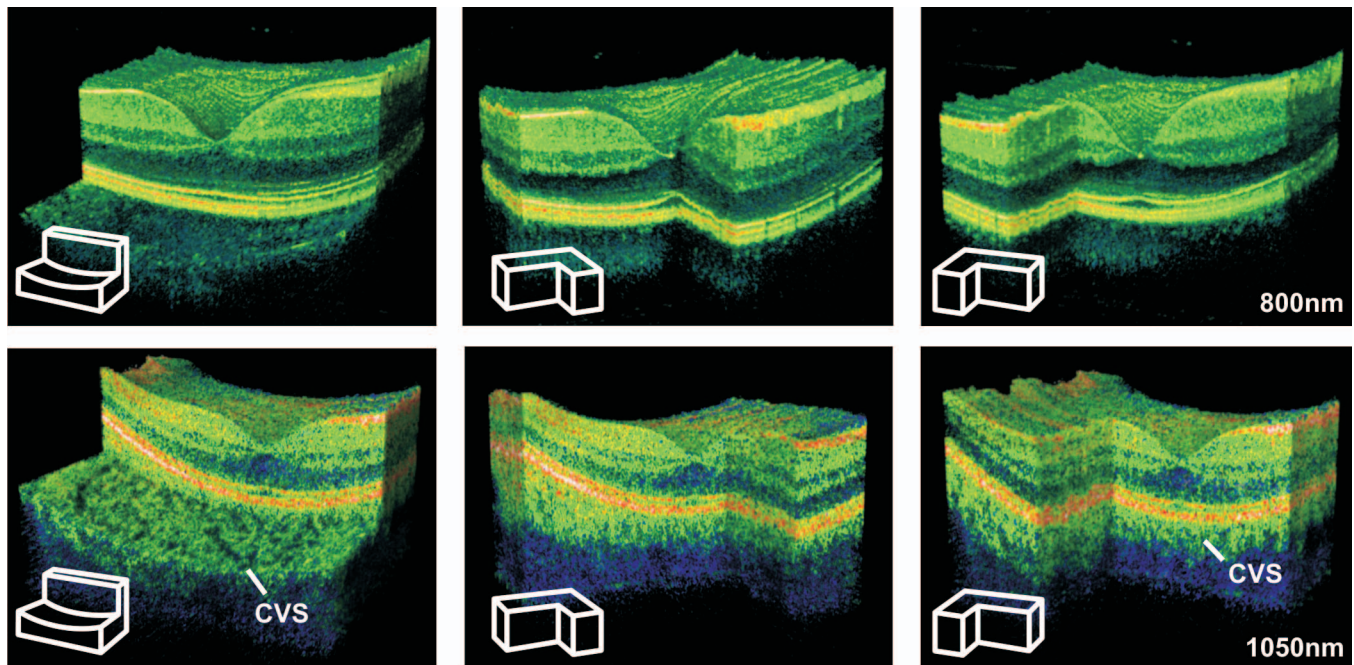


Fig. 2 Comparison of a normal retina (fovea at center) imaged at 800 nm (top) and 1050 nm (bottom). The choriovascular system (CVS) can be visualized only using 1050 nm.

neath the retinal pigment epithelium (RPE) as well as delineation of the choroidal structure. The ability to image at these depths with high resolution has major potential for early diagnosis of retinal disorders, such as neovascularization in age-related macular degeneration in which the earliest signs of pathology are likely to occur at the RPE-choroidal interface. Given the reduced scattering at longer wavelengths, we anticipate that images with this degree of penetration and quality can also be obtained in patients with clinically significant lens opacities. With the recent availability of novel broad bandwidth light sources and InGaAs-based CCD detectors, and widely tunable light sources for imaging at ~ 1050 nm, high-speed FD-OCT has the potential to become a clinically viable tool to increase our knowledge of the pathogenesis of pathologies affecting the outer retinal layers as well as providing the capacity for the early detection of diseases and the objective monitoring of any therapeutic interventions. Current light source technology favors broadband emitting sources, necessary to achieve high axial resolutions, over spectrally swept ones because of the exploitation of nonlinear broadening effects not available in tunable narrow linewidth emitters. Furthermore, ongoing camera and source development should help to improve sampling depth and acquisition speed. Time domain and spatially encoded FD-OCT can exploit these light sources. The sensitivity advantage of FD-OCT allows for high-speed 3-D scanning but involves challenges due to the imaging geometry of the broadband, high-speed spectrometer.

In this study, we present the first comparison of 3-D 1050 nm FD-OCT to a comparable 800 nm OCT system built upon the spectrometer-based operation scheme and demonstrate the clinical feasibility and performance advantages of using this novel OCT method to image retinal and choroidal structure in patients with cataract.

2 Methods

To enable 3-D *in vivo* retinal imaging at 1050 nm, an FD-OCT system has been developed employing an all-mirror-based, high-resolution, high-speed spectrometer using an InGaAs, 512 pixel line array camera (Sensors Unlimited, Inc., Princeton, New Jersey) with $25 \mu\text{m}$ pixel pitch, capable of 5 Msamples/s similar to a previously presented setup²² operating at 1300 nm. The source operated at 1045 nm with a bandwidth of 70 nm (1 micron ASE module, NP-Photonics, Inc., Tucson, Arizona) emitting more than 20 mW (ex fiber) and was fiber-optically linked to a 20/80 beamsplitter serving the sample arm and the reference arm, respectively (Fig. 1), enabling $\sim 7 \mu\text{m}$ axial resolution. The reference arm incorporated a free-space pathway and dispersion compensation material to balance fiber length mismatch and the dispersion of the human eye. The device was interfaced to a patient module (OCT-2, provided by Zeiss Meditec, Inc., Dublin, California), modified for operation at 1050 nm to enable clinical retinal imaging at this wavelength. The spectrometer itself was designed around a flat, reflective 1200 l/mm grating, blazed for $1.1 \mu\text{m}$ and completed with a gold-coated spherical collimation and focusing mirror, with 25 and 50 mm diameter and -200 and -500 mm radius of curvature, respectively, distributing and concentrating the light along the linear pixel array. The all-reflective approach was chosen to utilize readily available components and operates in a very compact geometry,

maximizing mechanical stability and minimizing internal chromatic aberrations. Electronic data were transferred by a standard CameraLink connection and acquired by a frame grabber that was connected to an external digital signal processor responsible for timing and control of the scanning galvanometric mirrors. The typical B-mode scan dimensions were 256 depth positions (512 sample points in the frequency domain) and 512 depth scans, enabling up to 20 frames/s. The alternative 800-nm system was built on the same platform (patient module, electronics and post processing) and used a lens and reflective grating based spectrometer, designed for 180 nm bandwidth together with a 2048 pixel (Atmel Aviiiva) line camera and a broadband Titanium:Sapphire laser (Femtolasers Integral, Vienna, Austria) emitting 52 mW with 160 nm bandwidth centered at 800 nm to achieve $\sim 3 \mu\text{m}$ axial resolution,¹⁰ acquiring 1024 depth-scans per cross section.

The exposure time per sample line was set to $43 \mu\text{s}$ at 800 nm and $52 \mu\text{s}$ at the 1050 nm system, to operate at comparable performance. Both systems were set up in parallel to allow for fast switching between the instruments and operated under optimal imaging conditions with ~ 95 dB sensitivity that was measured by comparison of the noise level to a previous calibration measurement at the same camera settings with a neutral filter of known density. The depth-dependent sensitivity loss that is common to spatially encoded OCT was found to be greater with the broadband spectrometer (-12 dB at half of the scanning range at 800 nm and -9 dB at 1050 nm). The scanning ranges were similar, despite the different spectral ranges, detector resolutions (2048 versus 512 elements), and spectral utilization of the detectors width (1.3 mm for the 800 nm device and 1.7 mm for the 1050 nm device). Aside from the typical effect of finite pixel size, this was mainly caused by limitations of the imaging geometry and cross talk between adjacent channels that increased the depth-dependent signal loss at higher pixel numbers and increased detector length and bandwidth. The effective axial resolutions for the systems at 800 nm were found to be $\sim 3 \mu\text{m}$ and $\sim 7 \mu\text{m}$ at 1050 nm. Measurements were taken close to the zero delay position—with the proximal part of the retina, the inner limiting membrane (ILM) oriented toward the higher SNR at the zero delay to allow for optimal and equal imaging conditions of both instruments and to avoid preference of one of the systems. After spectral resampling and Fourier transformation, the cross-sectional slices were shifted according to utilizing their cross-correlation to compensate motion artifacts along the slow scanning axis.

The study was approved by the Ethics Committee of the City of Vienna, Austria, and conducted according to the tenets of the Declaration of Helsinki (Final Revision: 52nd WMA General Assembly, Edinburgh, Scotland, 2000). Written and informed consent was obtained from all study participants after detailed explanation of the aims and risks of the study. Twenty-six eyes of 14 patients were imaged. Patients were known to have cataracts and pathological conditions affecting the RPE and adjacent structures. Cataract grades were determined by an experienced ophthalmologist using the LOCS III grading scheme.²⁶ All pupils were dilated to >5 mm using topical Tropicamide 1% (Mydraticum, Agepha) to provide sufficient parafoveal access to the retina at the different im-

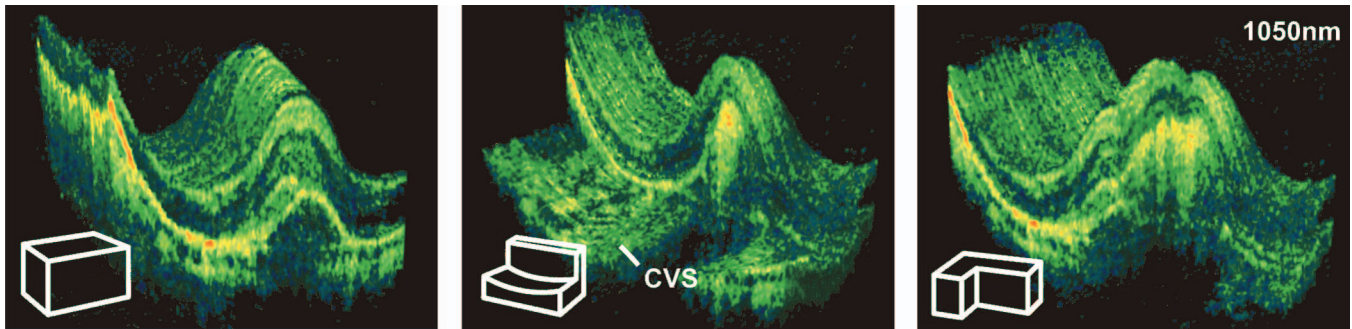


Fig. 3 Pathologic retina [age-related macular degeneration (AMD) and senile cataract] acquired with the 3-D 1050 nm OCT system. Multiple virtual cuts give insight of the 3-D structure of the hematoma located in the center of the volume and the associated chorioideo vascular system (CVS).

aging conditions. While 750 μ W of broadband radiation at 800 nm can easily be seen by the subject, light at 1050 nm was imperceptible even though it was delivered at higher power of up to 3.5 mW to compensate for water absorption losses in the vitreous. However, nonlinear effects in the light generation of the amplified spontaneous emission (ASE) source emitted a small portion additionally emitted $<10 \mu$ W of incident light at the margin of the visible light that could be used as a dim fixation light during the scan, alternative to external fixation of the other eye. All eyes were examined with the 1050-nm system, immediately after the 800-nm FD-OCT measurements.

3 Results and Discussion

Retinas were imaged with different scanning patterns, altering the transversal sampling range and orientation (horizontal or vertical) with both systems. The raster scans typically spanned regions about 1 to 3 times the foveal diameter (2 to 6 deg of visual field, equivalent to 1 to 3 mm) in a square field. The 800 nm system sampled in a 1024×60 grid, while the 1050 nm system resembled a 512×60 grid, permitting to simultaneously produce high-density scans within the full volume. Compared to normal subjects, the wide image sensitivity range of almost 40 dB (at ~ 95 dB absolute sensitivity in the usable image depth range, calibrated to a test measurement with an attenuated test sample) was reduced to less than 10 dB (~ 65 dB abs.) in eyes with advanced cataract where retinal reconstruction was impossible at 800 nm in the TD and FD systems. Fixation was more challenging using the faint visible portion of light emitted from the ASE source of the 1050 nm device compared with the bright fixation spot in the 800 nm system. In some cases, external fixation with the other eye, in the 1050 nm or even in both systems, had to be used.

With cataract patients, the 1050 nm system provided a significantly higher SNR, which facilitated the investigation of intraretinal structures, despite optical scattering in the beam path. Figure 2 shows a comparison of 3-D rendered retinal volume with virtual sections for the same region of interest in a normal healthy subject without cataract. From these images, it is clear that the depth-dependent intensity characteristics at the two wavelengths are not equal, as seen with time domain and time-encoded frequency domain OCT systems in previous studies.^{19,24} While producing comparable peak signals within

the depth scans, the individual deeper layers have different relative intensity, in addition to the different wavelength-dependent penetration. However, the degrees of backscattering at the level of the RPE are comparable in the two measurements, indicating a low influence of wavelength-independent system parameters (i.e., FD-OCT typical depth-dependent sensitivity loss for $\sim 250 \mu$ m of retinal thickness is similar). As described in a previous article,¹⁹ multiple wavelength-dependent effects play a role when comparing the intensity values, including backscattering decrease and increase of specific layers and the lower depth-dependent dispersion at 1050 nm. The lower transverse sampling (512 depth-scans/frame at 1050 nm versus 1024 depth-scans/frame at 800 nm) and axial resolution of the 1050 nm system reduce the contrast of subtle details of intraretinal structure. Nevertheless, for retinal layers beneath the RPE such as the choriocapillaris and superficial parts of the choroid, the visualization of the anatomical microstructure is improved in respect to the 800 nm case, and individual lumina of the choroidal vessels can be visualized. Similar differences in the two imaging modalities can be noticed in patients with retinal diseases. A patient with age-related macular degeneration (AMD) and cataract could be imaged with the 1050 nm OCT

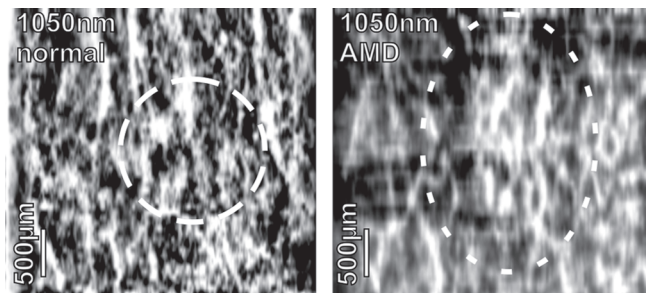


Fig. 4 Topographically mapped *en face* view of the chorioideo vascular system (CVS) (2.5×2.5 mm) detected by 3-D OCT at 1050 nm in a normal subject (left, same dataset as in Fig. 2) and an advanced cataract patient with AMD (right, same set as Fig. 3). Lower backreflection due to vessels is presented in white. Despite the cataract that reduces the image quality, choroidal vasculature can be visualized by 3-D OCT at 1050 nm, indicating increase of vessel density at the center of the choroidal neovascularization area, depicted by a dotted circle in respect to the surroundings and the foveal region in the normal (dashed ellipse).

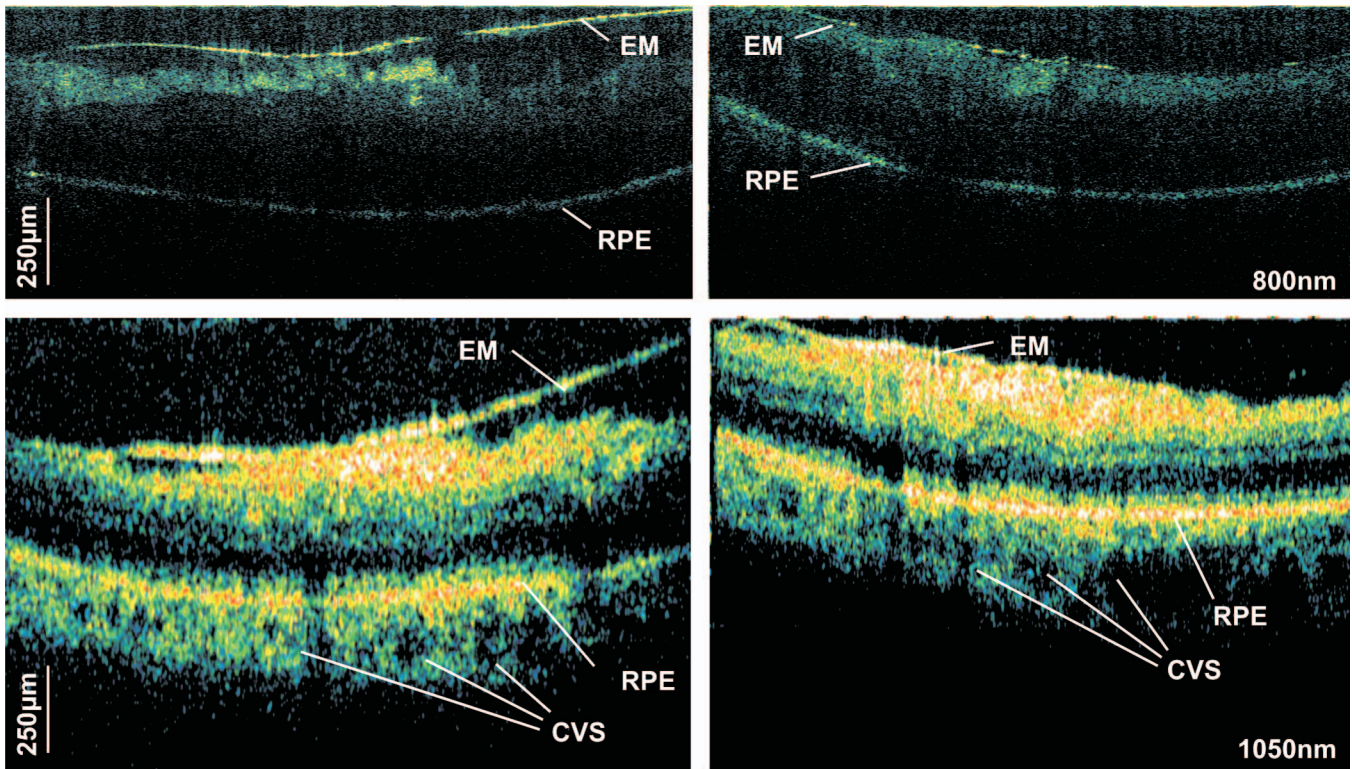


Fig. 5 Comparison of OCT cross sections of a pathologic retina (macular pucker), acquired through a cataract (LOCS: N04 NC4) at 800 nm (top row) and 1050 nm (bottom row). The retinal pigment epithelium (RPE) and epiretinal membrane (EM) are indicated. Overall signal quality is strongly improved, and at the bottom of the tomograms, the choroideo vascular system (CVS) is visible only when imaging at 1050 nm.

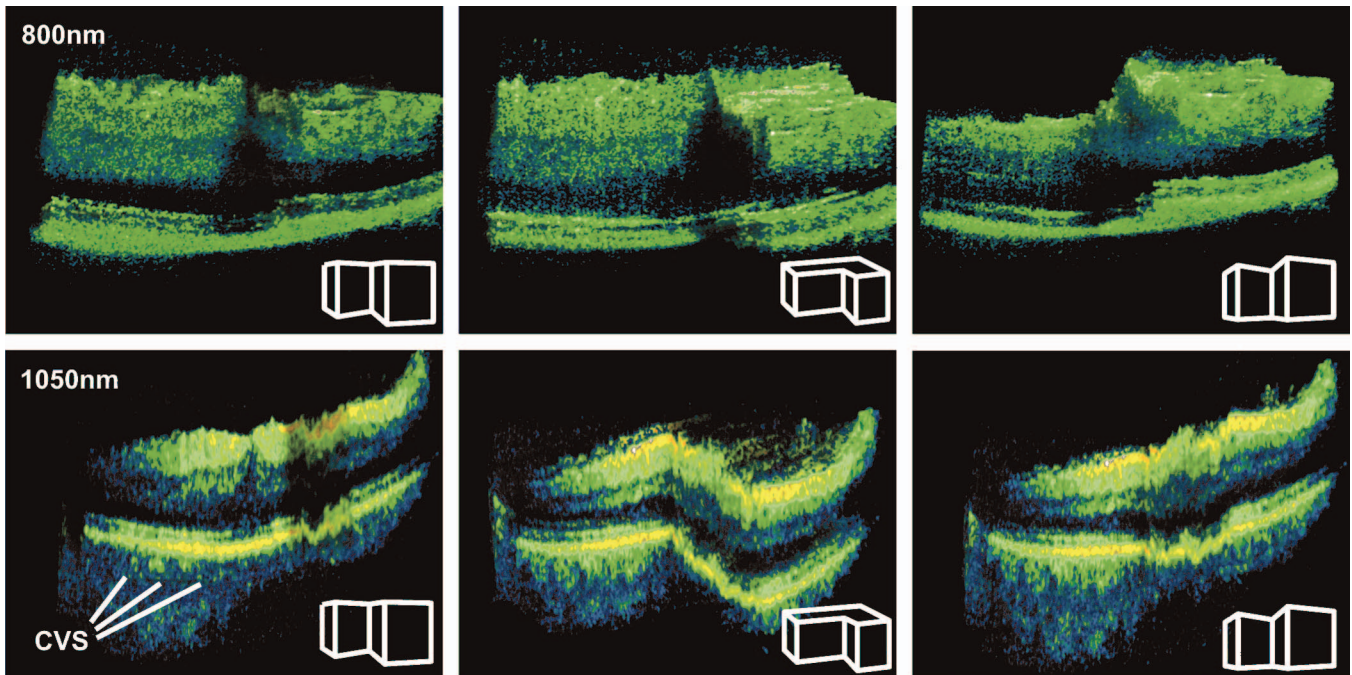


Fig. 6 Three-dimensional rendering of a retina with macular pucker and cataract (LOCS III: N01.5 NC1.5 C2.2 P3.0) imaged at 800 and 1050 nm at the same site, demonstrating the effects of lower scattering by the cataract and simultaneous higher penetration beyond the retinal pigment epithelium (RPE) into the choroideo vascular system (CVS) in the case of the longer wavelength. The 800 nm tomograms lack of contrast is due to much lower signal intensity and therefore low signal to noise ratio (SNR).

system (Fig. 3), while the 800 nm system failed to identify more than the RPE. Despite the present cataract, the outer retinal structure and inner choroidal structure can clearly be visualized, although the lower resolution and sampling interval reduces the overall image quality and ability to resolve details.

Deeper penetration into the choroid despite cataract is demonstrated in Fig. 4, where the RPE is used as a boundary for segmentation of the choroid. Selection of a choroidal slice in the 3-D dataset and successive integration along the depth results in visualization of the choroidal vessel system beneath the retina, shown for the normal subject [Fig. 4(a)] cataract patient with AMD [Fig. 4(b)]. The altered distribution of vessel reflectivity in the central region and relative lower signal in its elliptic circumference coincides with the abnormal retinal structure seen in Fig. 3. It has to be pointed out that the tomograms were acquired in an orientation that allows monitoring of all retinal layers in one measurement with the higher SNR at the ILM, rather than close to the RPE. To further enhance the signal in the choroid, the OCT zero-delay plane could be placed on the other side; this however would deteriorate the signal on the more proximal retinal structure. The latter would be acceptable in the normal case but could not be used to investigate the extended pathologic structure in Fig. 3.

In Fig. 5, 3-D OCT imaging at 800 nm (top) and 1050 nm (bottom) of a patient with an epiretinal membrane and macular pucker is depicted. The imaging sensitivity has been significantly reduced by the presence of moderately advanced cataract (LOCS: N04 NC4) when using the 800 nm OCT system. The effect of the cataract varied as a function of the scan angle in some cases, markedly reducing contrast in the 800 nm tomogram and effectively obscuring any details of retinal structure. When the same retina was imaged at 1050 nm, sufficient imaging sensitivity allowed perceiving the details of the intraretinal structure. The increase in image pixelation and speckle arises in the 1050 nm image from lower transverse sampling and resolution.

Differences in the light scattering properties of the cataract can have a significant impact on the quality of the image. In Fig. 6, the lens opacity would be expected to have a greater light scattering effect because of the presence of significant posterior subcapsular opacity (LOCS III: NO1.5 NC1.5 C2.2 P3.0). The image obtained at 800 nm has sufficient signal strength to allow for 3-D imaging. However, the image obtained at 1050 nm provides considerably more detail of retinal structure and reveals puckering of the retinal surface with preservation of the integrity of the deeper retinal layers.

4 Conclusions

In this study, we have demonstrated that the performance of 800 nm FD-OCT systems is significantly affected by light scattering induced by cataract. By contrast, light scattering with 1050 nm OCT systems is noticeably less and provides better delineation of retinal structure. It should be emphasized that the present study was designed to evaluate the principle of retinal imaging at longer wavelengths in patients with cataract and retinal pathologies and therefore does not provide a detailed analysis of the effects of different types of lens opacity on OCT images. *A priori*, we would expect less of an effect with nuclear opacities (e.g., nuclear sclerosis) compared

with the greater scattering effects of cortical or subcapsular opacities.²⁷ A more detailed analysis of this type is the subject of further investigation.

The better performance in cataract patients of the 1050 nm OCT system suggests that it has a place in the clinical assessment of retinal structure. For the analysis of diseases that affect the outer retina and choroid, the great depth penetration that can be achieved with this modality suggests that it will be of value in the early diagnosis of similar conditions and in monitoring the effects of treatment. For example, some of the earliest signs of AMD can be observed at the level of Bruch's membrane and adjacent choriocapillaries.²⁸

Diabetic retinopathy is also associated with a change in the choroidal vascularization and with increased deposition of laminar deposits in Bruch's membrane that are not readily apparent with routine clinical examination techniques.²⁹ It is possible that imaging at longer wavelengths may also be beneficial in the assessment of glaucomatous optic neuropathy, possibly allowing analysis of the structural changes within the lamina cribrosa that have, clinically, been restricted to the surface layers of this structure.^{24,30} Longer wavelengths may also be useful in the assessment of anterior segment structures. OCT can monitor changes in corneal thickness with great accuracy and may therefore be valuable in the assessment of laser ablative techniques used in refractive surgery where 1050 nm light sources might also replace sources operating at 1.3 μm .³¹

Last, since the longer wavelengths do not stimulate the retina, they can be used to probe the effects of retinal stimulation by other, shorter and more visible wavelengths. We have already demonstrated that OCT can be used to detect physiological correlates of neuronal activity^{32,33} within the retina, and we see the use of these longer wavelengths as a way of separating the processes of stimulation and neuronal recording at the same point in the retina.

In summary, using 1050 nm light sources, we have observed significant improvements in the quality of OCT images obtained in eyes with turbid media. Combined with the advantage of greater depth penetration into the choroid, we anticipate that this imaging modality will become a valuable clinical tool in early assessment, staging, and therapeutic monitoring of retinal disease.

Acknowledgments

Support for this project was provided by the following institutions: Cardiff University, FP6-IST-NMP-2 STREPT (017128), FWF Y 159-PAT, the Christian Doppler Society, NP Photonics (Tucson, Arizona), FEMTOLASERS GmbH (Vienna, Austria), Carl Zeiss Meditec, Inc. (Dublin, California), and Maxon Computer GmbH (Friedrichsdorf, Germany).

References

1. A. F. Fercher, C. K. Hitzenberger, G. Kamp, S. Y. El-Zaiat, K. Seta, and B. K. Ward, "Measurement of intraocular distances by back-scattering spectral interferometry: interferometric absolute distance measurement utilizing a mode-jump region of a laser diode," *Opt. Commun.* **117**, 43–48 (1995).
2. G. Häusler and M. W. Lindner, "'Coherence radar' and 'Spectral Radar'—new tools for dermatological diagnosis," *J. Biomed. Opt.* **3**, 21–31 (1998).

3. R. Leitgeb, C. K. Hitzenberger, and A. F. Fercher, "Performance of Fourier domain vs. time domain optical coherence tomography," *Opt. Express* **11**(8), 889–894 (2003).
4. M. A. Choma, M. V. Sarunic, C. H. Yang, and J. A. Izatt, "Sensitivity advantage of swept source and Fourier domain optical coherence tomography," *Opt. Express* **11**(18), 2183–2189 (2003).
5. J. F. de Boer, B. Cense, B. H. Park, M. C. Pierce, G. J. Tearney, and B. E. Bouma, "Improved signal-to-noise ratio in spectral-domain compared with time-domain optical coherence tomography," *Opt. Lett.* **28**(21), 2067–2069 (2003).
6. N. A. Nassif, B. Cense, B. H. Park, M. C. Pierce, S. H. Yun, B. E. Bouma, G. J. Tearney, T. C. Chen, and J. F. de Boer, "In vivo high-resolution video-rate spectral-domain optical coherence tomography of the human retina and optic nerve," *Opt. Express* **12**(3), 367–376 (2004).
7. R. A. Leitgeb, W. Drexler, A. Unterhuber, B. Hermann, T. Bajraszewski, T. Le, A. Stingl, and A. F. Fercher, "Ultra-high resolution Fourier domain optical coherence tomography," *Opt. Express* **12**(10), 2156–2165 (2004).
8. M. Wojtkowski, V. J. Srinivasan, T. H. Ko, J. G. Fujimoto, A. Kowalczyk, and J. S. Duker, "Ultra-high-resolution, high-speed, Fourier domain optical coherence tomography and methods for dispersion compensation," *Opt. Express* **12**(11), 2404–2422 (2004).
9. B. Cense and N. A. Nassif, "Ultra-high-resolution high-speed retinal imaging using spectral-domain optical coherence tomography," *Opt. Express* **12**(11), 2435–2447 (2004).
10. U. Schmidt-Erfurth, R. A. Leitgeb, S. Michels, B. Pivažay, S. Sacu, B. Hermann, C. Ahlers, H. Sattmann, C. Scholda, A. F. Fercher, and W. Drexler, "Three-dimensional ultra-high-resolution optical coherence tomography of macular diseases," *Invest. Ophthalmol. Visual Sci.* **46**(9), 3393–3402 (2005).
11. V. J. Srinivasan, M. Wojtkowski, A. J. Witkin, J. S. Duker, T. H. Ko, M. Carvalho, J. S. Schuman, A. Kowalczyk, and J. G. Fujimoto, "High-definition and 3-dimensional imaging of macular pathologies with high-speed ultra-high-resolution optical coherence tomography," *Ophthalmology* **113**(11), 2051–2014 (2006).
12. D. Huang, E. A. Swanson, C. P. Lin, J. S. Schuman, W. G. Stinson, W. Chang, M. R. Hee, T. Flotte, K. Gregory, C. A. Puliafito, and J. G. Fujimoto, "Optical coherence tomography," *Science* **254**(5035), 1178–1181 (1991).
13. M. R. Hee, J. A. Izatt, E. A. Swanson, D. Huang, J. S. Schuman, C. P. Lin, C. A. Puliafito, and J. G. Fujimoto, "Optical coherence tomography of the human retina," *Arch. Ophthalmol. (Chicago)* **113**(3), 325–332 (1995).
14. C. A. P. J. S. Schuman and J. G. Fujimoto, *Optical Coherence Tomography of Ocular Disease*, Slack Inc., Thorofare, NJ (2004).
15. W. Drexler, U. Morgner, R. K. Ghanta, F. X. Kartner, J. S. Schuman, and J. G. Fujimoto, "Ultra-high-resolution ophthalmic optical coherence tomography," *Nat. Med.* **7**(4), 502–507 (2001).
16. W. Drexler, H. Sattmann, B. Hermann, T. H. Ko, M. Stur, A. Unterhuber, C. Scholda, O. Findl, M. Wirtitsch, J. G. Fujimoto, and A. F. Fercher, "Enhanced visualization of macular pathology with the use of ultra-high-resolution optical coherence tomography," *Arch. Ophthalmol. (Chicago)* **121**(5), 695–706 (2003).
17. T. H. Ko, J. G. Fujimoto, J. S. Duker, L. A. Paunescu, W. Drexler, C. R. Baumal, C. A. Puliafito, E. Reichel, A. H. Rogers, and J. S. Schuman, "Comparison of ultra-high- and standard-resolution optical coherence tomography for imaging macular hole pathology and repair," *Ophthalmology* **111**(11), 2033–2043 (2004).
18. L. Hyman, S. Y. Wu, A. M. Connell, A. Schachat, B. Nemesure, A. Hennis, and M. C. Leske, "Prevalence and causes of visual impairment in the Barbados Eye Study," *Ophthalmology* **108**(10), 1751–1756 (2001).
19. A. Unterhuber, B. Považay, B. Hermann, H. Sattmann, A. Chavez-Pirson, and W. Drexler, "In vivo retinal optical coherence tomography at 1040-nm enhanced penetration into the choroid," *Opt. Express* **13**(9), 3252–3258 (2005).
20. A. N. S. Institute, "Safe use of lasers," ANSI Z136.1–2000, American National Standards Institute, p. 173 (2000).
21. I. C. o. N.-I. R. Protection, "Revision of guidelines on limits of exposure to laser radiation of wavelengths between 400 nm and 1.4 μm ," *Health Phys.* **79**(9), 431–440 (2002).
22. S. H. Yun, G. J. Tearney, B. E. Bouma, B. H. Park, and J. F. de Boer, "High-speed spectral-domain optical coherence tomography at 1.3 μm wavelength," *Opt. Express* **11**(26), 3598–3604 (2003).
23. B. Považay, K. Bizheva, B. Hermann, A. Unterhuber, H. Sattmann, A. F. Fercher, W. Drexler, C. Schubert, P. K. Ahnelt, M. Mei, R. Holzwarth, W. J. Wadsworth, J. C. Knight, and P. S. Russel, "Enhanced visualization of choroidal vessels using ultra-high resolution ophthalmic OCT at 1050 nm," *Opt. Express* **11**(17), 1980–1986 (2003).
24. E. C. Lee, J. F. de Boer, M. Mujat, H. Lim, and S. H. Yun, "In vivo optical frequency domain imaging of human retina and choroid," *Opt. Express* **14**, 4403–4411 (2006).
25. J. Zhang, Q. Wang, B. Rao, Z. Chen, and K. Hsu, "Swept laser source at 1 μm for Fourier domain optical coherence tomography," *Appl. Phys. Lett.* **89**, 073901 (2006).
26. L. T. Chylack Jr., J. K. Wolfe, D. M. Singer, M. C. Leske, M. A. Bullimore, I. L. Bailey, J. Friend, D. McCarthy, and S. Y. Wu, "The lens opacities classification system III. The longitudinal study of cataract study group," *Arch. Ophthalmol. (Chicago)* **111**(6), 831–836 (1993).
27. M. E. van Velthoven, M. H. van der Linden, M. D. de Smet, D. J. Faber, and F. D. Verbraak, "Influence of cataract on optical coherence tomography image quality and retinal thickness," *Br. J. Ophthalmol.* **90**(10), 1259–1262 (2006).
28. G. Luttj, J. Grunwald, A. B. Majji, M. Uyama, and S. Yoneya, "Changes in choriocapillaries and retinal pigment epithelium in age-related macular degeneration," *Mol. Vis* **5**, 35 (1999).
29. J. Cao, S. McLeod, C. A. Merges, and G. A. Luttj, "Choriocapillaris degeneration and related pathologic changes in human diabetic eyes," *Arch. Ophthalmol. (Chicago)* **116**(5), 589–597 (1998).
30. A. Bhandari, L. Fontana, F. W. Fitzke, and R. A. Hitchings, "Quantitative analysis of the lamina cribrosa in vivo using a scanning laser ophthalmoscope," *Curr. Eye Res.* **16**(1), 1–8 (1997).
31. F. Memarzadeh, Y. Li, B. A. Francis, R. E. Smith, J. Gutmark, and D. Huang, "Optical coherence tomography of the anterior segment in secondary glaucoma with corneal opacity after penetrating keratoplasty," *Br. J. Ophthalmol.* **91**(2), 189–192 (2007).
32. K. Bizheva, R. Pflug, B. Hermann, B. Považay, H. Sattmann, P. Qiu, E. Anger, H. Reitsamer, S. Popov, J. R. Taylor, A. Unterhuber, P. Ahnelt, and W. Drexler, "Optophysiology: depth-resolved probing of retinal physiology with functional ultra-high-resolution optical coherence tomography," *Proc. Natl. Acad. Sci. U.S.A.* **103**(13), 5066–5071 (2006).
33. V. J. Srinivasan, M. Wojtkowski, J. G. Fujimoto, and J. S. Duker, "In vivo measurement of retinal physiology with high-speed ultra-high-resolution optical coherence tomography," *Opt. Lett.* **31**(15), 2308–2310 (2006).